University of Nebraska - Lincoln

DigitalCommons@University of Nebraska - Lincoln

Xiao Cheng Zeng Publications

Published Research - Department of Chemistry

5-1-2006

Search for global-minimum geometries of medium-sized germanium clusters. II. Motif-based low-lying clusters Ge$_{21}$–Ge$_{29}$

S. Yoo
University of Nebraska-Lincoln

Xiao Cheng Zeng
University of Nebraska-Lincoln, xzeng1@unl.edu

Follow this and additional works at: https://digitalcommons.unl.edu/chemzeng

Part of the Chemistry Commons

Yoo, S. and Zeng, Xiao Cheng, "Search for global-minimum geometries of medium-sized germanium clusters. II. Motif-based low-lying clusters Ge$_{21}$–Ge$_{29}$" (2006). *Xiao Cheng Zeng Publications*. 8.
https://digitalcommons.unl.edu/chemzeng/8

Search for global-minimum geometries of medium-sized germanium clusters. II. Motif-based low-lying clusters Ge$_{21}$–Ge$_{29}$

S. Yoo and X. C. Zeng[a)]

Department of Chemistry, University of Nebraska-Lincoln, Lincoln, Nebraska 68588

We performed a constrained search for the geometries of low-lying neutral germanium clusters Ge$_N$ in the size range of $21 \leq N \leq 29$. The basin-hopping global optimization method is employed for the search. The potential-energy surface is computed based on the plane-wave pseudopotential density functional theory. A new series of low-lying clusters is found on the basis of several generic structural motifs identified previously for silicon clusters [S. Yoo and X. C. Zeng, J. Chem. Phys. **124**, 054304 (2006)] as well as for smaller-sized germanium clusters [S. Bulusu *et al.*, J. Chem. Phys. **122**, 164305 (2005)]. Among the generic motifs examined, we found that two motifs stand out in producing most low-lying clusters, namely, the *six/nine* motif, a puckered-hexagonal-ring Ge$_6$ unit attached to a tricapped trigonal prism Ge$_9$, and the *six/ten* motif, a puckered-hexagonal-ring Ge$_6$ unit attached to a bicapped antiprism Ge$_{10}$. The low-lying clusters obtained are all prolate in shape and their energies are appreciably lower than the near-spherical low-energy clusters. This result is consistent with the ion-mobility measurement in that medium-sized germanium clusters detected are all prolate in shape until the size $N \sim 65$. © *2006 American Institute of Physics.*
[DOI: 10.1063/1.2192783]

I. INTRODUCTION

Among main group-IV elements, silicon and germanium have many properties in common. For example, both are semiconductors in cubic diamond form. Moreover, the global-minimum silicon clusters Si$_N$ and germanium clusters Ge$_N$ have identical geometries up to $N=12$.[1] In the size range of $13 \leq N \leq 20$, although the growth patterns of many silicon clusters differ from those of germanium clusters,[1,2] a majority of low-lying silicon and germanium clusters still contain a common structural motif, namely, the *tricapped trigonal prism* (TTP) motif.[3] In our previous study of germanium clusters in the size range of $16 \leq N \leq 20$ (Paper I of this series[2]), we examined the second generic structural motif, namely, the so-called six/six motif[4]—a puckered-hexagonal-ring Ge$_6$ unit attached to a tetragonal bipyramid Ge$_6$. We found that some energetically competitive germanium clusters can be also built based on the six/six motif, such as Ge$_{19}$. For silicon clusters, a TTP-to-six/six motif transition has been predicted to occur in the size range of Si$_{16}$ to Si$_{18}$.[4–7] However, for germanium clusters, the TTP motif dominates the population of the lowest-energy clusters in the size range of $10 \leq N \leq 20$, while the six/six motif plays a lesser role.

The silicon clusters in the size range of $21 \leq N \leq 29$ have received considerable attention over the past five years,[4,8–17] largely because previous ion-mobility experiments[18,19] showed that a structural transition from prolate to near-spherical geometries occurs at $N=27\pm2$ for both cation and anion silicon clusters. In contrast, for cation germanium clusters, previous ion-mobility experiments showed that the prolate-to-near-spherical transition does not occur until

$N \sim 65$.[20] Thus, it is expected that the growth pathway of silicon and germanium clusters would differ more from each other beyond the size range of $N=27–29$. Undoubtedly, if the geometries of lowest-energy germanium clusters in the size range of $21 \leq N \leq 29$ are known, it will help us to gain better insight into the structural evolution of small-sized clusters towards nanocrystalline quantum dots[21] as well as to understand why the growth pathway of the two group-IV clusters starts to show major deviation beyond $N=29$. For the latter purpose, we first summarize some generic structural features of lowest- and low-lying silicon clusters in the size range of $21 \leq N \leq 30$. These features have been revealed by many researchers via either unbiased or constrained global searches in conjunction with either semiempirical tight-binding or the first-principles density functional theory (DFT) calculations of the potential-energy surface.[9,10,12,13,17] Briefly, nearly all the low-lying silicon clusters in the size range of $21 \leq N \leq 30$ can be classified into four distinct structural families:[17] (1) Clusters in the first family can be assembled by connecting two small-sized "magic-number" clusters Si$_N$ ($N=6$, 7, 9, or 10) with a fused-puckered-hexagonal-ring Si$_9$ unit (a fragment of bulk diamond silicon) in between; (2) clusters in the second family can be constructed on the basis of a structural motif consisting of a puckered-hexagonal-ring Si$_6$ and small-sized magic-number clusters Si$_N$ ($N=6$, 7, 9, and 10), that is, the six/six, *six/seven*, *six/nine*, or *six/ten* motif; (3) clusters in the third family are near spherical cagelike in geometry, and many can be viewed as homologue to the endohedral carbon fullerenes;[12] and (4) clusters in the fourth family are Y-shaped "three-arm" clusters, in which the three arms are the small-sized magic clusters and the "glue" unit is structurally similar to the fused-puckered-hexagonal-ring Si$_9$ unit.

a)Electronic mail: xczeng@phase2.unl.edu

The purpose of this paper is to examine relative stability of those low-lying germanium clusters with structures homologues to the four silicon structural families discussed above. We noticed that compared to the silicon clusters, much less theoretical studies have been devoted to the structures of low-lying germanium clusters.[1,2,22–24] To our knowledge, only two papers in the literature show geometric structures of low-lying Ge$_N$ in the size range of $21 \leqslant N \leqslant 29$. Wang *et al.* reported candidates for lowest-energy clusters up to $N=25$, based on a global search using the genetic algorithm (GA) coupled with a nonorthogonal tight-binding (NTB) model.[23] They found that for Ge$_N$ ($N>13$), the stacked layered structures and the spherical-like compact structures compete for the lowest-energy structures. Later, Liang and Li studied geometric structures and electronic properties of medium-sized clusters Ge$_N$ ($21 \leqslant N \leqslant 25$) using a full-potential linear-muffin-tin-orbital molecular-dynamics (FP-LMTO-MD) method.[24] They suggested that low-lying prolate clusters can be built upon stacked TTP motifs. In this work, we combined the basin-hopping global optimization method with DFT calculation of the potential-energy surface. This combined computational approach coupled with many structural motifs identified previously allows us to obtain many new low-lying clusters with energy appreciably lower than the corresponding isomers reported previously.[22–25]

II. METHOD

We used the basin-hopping global optimization method to search for the geometries of low-lying clusters. The basin-hopping (BH) method has been applied to the Lennard-Jones clusters[26–28] as well as other atomic and molecular clusters.[27,29–32] Here we briefly summarize the BH global optimization technique. Details of this technique can be found elsewhere.[26,27,33] A key idea of the BH method is that the transformed potential-energy surface (PES) $\tilde{U}$ can be generated via the mapping

$$\tilde{U}(N,\mathbf{r}_1,\mathbf{r}_2,\ldots,\mathbf{r}_N) = \mathbf{min}\{U(N,\mathbf{r}_1,\mathbf{r}_2,\ldots,\mathbf{r}_N)\}, \qquad (1)$$

where **min** denotes the energy minimization performed with starting configuration of $\{\mathbf{r}_1,\cdots,\mathbf{r}_N\}$ and U is the PES. The topography of the transformed PES resembles a multidimensional staircase where each step corresponds to the basin of attraction. The basin of attraction represents a set of geometries from which the energy minimization always leads to the local minimum. By removing the intra-potential-well vibration, the system can "hop" directly between local minima at each step.

In practice, $\tilde{U}$ can be explored via canonical Monte Carlo (MC) simulation. For example, at each MC trial all movable coordinates are randomly displaced with an adjustable step size to yield an acceptance ratio of 0.5. The energy change $\Delta\tilde{U}$ for hopping between two minima is accepted with the probability of $\exp(-\Delta\tilde{U}/k_BT)$. In our previous study of smaller germanium clusters[2] (Paper I), we found that by directly coupling the BH method with the density functional calculation of the PES, we can generate low-lying clusters with energy appreciably lower than those reported previously
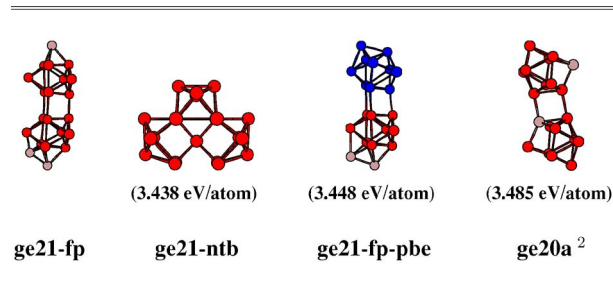

(3.438 eV/atom)   (3.448 eV/atom)   (3.485 eV/atom)

ge21-fp   ge21-ntb   ge21-fp-pbe   ge20a [2]

FIG. 1. (Color online) Geometries of two lowest-energy Ge$_{21}$ clusters previously reported: ge21-fp (Ref. 24) and ge21-ntp (Ref. 23). The cluster ge21-fp-pbe is obtained via a geometric optimization based on DFT/PBE calculation with the ge21-fp as the initial structure. The binding energies per atom (shown in parentheses) are based on the DFT/PBE calculation. The TTP Ge$_9$ motif and the bicapped antiprism Ge$_{10}$ motif are highlighted in red and blue, respectively. To compare the binding energy per atom, the lowest-energy cluster Ge$_{20}$ (Ref. 2) is also displayed.

based on semiempirical tight-binding model.[23] Here, we used the plane-wave-basis pseudopotential method with two popular exchange-correlation functionals within the general gradient approximation (GGA)—the Perdew-Burke-Ernzerhof (PBE) functional[34] and the BLYP functional[35]—implemented in the CPMD code.[36] We chose the norm-conserving nonlocal pseudopotential[37] constructed in the scheme of Troullier and Martins as a separable form of that of Kleinman-Bylander.[38,39] Initially, the constrained global search was done with less accurate PES for which a relatively small super-cell-size (20 Å) and plane-wave cutoff (15 Ry) were used. Once the top-five low-lying isomers were generated, their geometric structures were reoptimized by using a larger super-cell-size (25 Å) and plane-wave cutoff (30 Ry). No symmetry constraint was enforced during the geometry optimization.

Since DFT calculation of the PES demands much more computational time than the tight-binding calculations, a full (unbiased) global search for germanium clusters with size $N \geqslant 20$ becomes nearly impractical with our current computer facility. As shown previously,[4] if some generic structural motifs can be identified from smaller low-lying clusters, motif-based (constrained) global search can greatly reduce the computational time. In practice, the structure of the motif can be fixed while only remaining atoms of the clusters are subject to the MC trial move. However, we can no longer claim the lowest-energy clusters obtained from the constrained search as the global minima.

III. RESULTS AND DISCUSSION

First, we have examined binding energies per atom of two previously reported lowest-energy Ge$_{21}$ clusters, one obtained based on the combined genetic algorithm/NTB search[23] and another obtained via FP-LMTO-MD simulation.[24] Both global searches suggested that the lowest-energy Ge$_{21}$ cluster should contain the TTP motif. The two candidates for the global minimum of Ge$_{21}$ are shown in Fig. 1 where the cluster based on the FP-LMTO-MD calculation is denoted as ge21-fp and the one based on the NTB calculation is denoted as ge21-ntb. Both clusters contain the TTP motifs (highlighted in red). We reoptimized geometric struc-

TABLE I. Calculated energy differences with respect to the corresponding lowest-energy clusters (denoted by the boldfaced value **0.000**). Binding energy per atom (in eV/atom) of the lowest-energy clusters is given in parentheses. Those isomers whose energy-difference value from the lowest-energy isomer is less than 0.1 eV are considered to be isoenergetic with the lowest-energy cluster and their energies are also highlighted in boldface.

	PBE (eV)	BLYP (eV)
ge21-1a	**0.098**	**0.000** (3.177)
ge21-2a	**0.000** (3.476)	0.167
ge21-2b	0.160	0.185
ge21-ntb	0.793	1.041
ge22-1a	0.481	0.131
ge22-2a	**0.000** (3.487)	**0.000** (3.178)
ge22-2b	**0.022**	**0.029**
ge22-ntb	1.816	2.113
ge23-1a	0.887	0.531
ge23-2a	**0.000** (3.495)	**0.010**
ge23-2b	**0.005**	**0.000** (3.188)
ge23-2c	0.111	**0.029**
ge23-ntb	1.438	1.665
ge24-1a	0.358	0.367
ge24-2a	**0.000** (3.449)	**0.000** (3.197)
ge24-2b	0.210	0.355
ge24-ntb	1.463	1.807
ge25-1a	**0.001**	**0.000** (3.198)
ge25-2a	**0.000** (3.503)	0.144
ge25-2b	**0.070**	0.194
ge25-ntb	1.812	2.392
ge26-1a	0.390	0.171
ge26-2a	**0.000** (3.511)	**0.000** (3.200)
ge26-3a	1.079	1.712
ge26-4a	0.969	0.640
ge27-1a	**0.000** (3.494)	**0.000** (3.184)
ge27-1b	0.366	0.206
ge27-3a	0.779	1.415
ge27-4a	0.647	0.297
ge28-1a	**0.000** (3.509)	**0.000** (3.199)
ge28-3a	1.324	2.0016
ge28-4a	1.381	1.066
ge29-1a	**0.000** (3.524)	**0.000** (3.212)
ge29-3a	1.725	2.575
ge29-4a	1.032	0.848

tures of both ge21-fp and ge21-ntb using the PBE functional. The geometry of ge21-fp undergoes a notable change—the capped TTP subunit is converted into Ge_{10} bicapped antiprism[40] as shown in blue for ge21-fp-pbe (Fig. 1). Our DFT/PBE calculation indicates that both low-lying clusters have binding energy per atom about 0.037–0.047 eV/atom less than the proposed global-minimum cluster ge20a reported in Ref. 2, indicating that the two low-lying isomers are not the global minimum. Furthermore, as shown in Table I (see below), a newly obtained lowest-energy cluster (ge21-2a) is 0.793 eV lower in energy than ge21-ntb.

In Fig. 2 we display representative clusters examined in this study. As discussed in the Introduction, our main focus is placed on four distinct structural families (which have been previously studied for the silicon counterparts[17]): (1) Prolate clusters in family I can be assembled by connecting two small-sized magic-number clusters—either the *tetragonal bipyramid* Ge_6 (yellow), *pentagonal bipyramid* Ge_7

(light-purple), TTP Ge_9 (red), or *bicapped antiprism* Ge_{10} (blue)—via a *fused-puckered-hexagonal-ring* Ge_9 unit (green); (2) prolate clusters in family II can be constructed on the basis of a structural motif consisting of a *puckered-hexagonal-ring* Ge_6 (green) and small-sized magic-number clusters Ge_N ($N=6$, 7, 9, and 10), that is, either the six/six, *six/seven*, *six/nine*, or *six/ten* motif; (3) near-spherical clusters in family III are endohedral cagelike clusters (endohedral atoms are in blue);[12] and (4) clusters in family IV are "handmade" Y-shaped three-arm clusters, in which the three arms are the small-sized clusters (Ge_6–Ge_9) and the glue unit (in green) is structurally similar to the fused-puckered-hexagonal-ring Ge_9 unit. In Fig. 2, we also used the same cluster notation as before,[17] where the notation 1a refers to the isomer that has the lowest (PBE) energy in family I and the notation 1b refers to the isomer that has the second lowest energy in family I. In Table I, we list the binding energies per atom of the lowest-energy clusters and the energy difference between all clusters with respect to the lowest-energy clusters. It can be seen that the binding energies per atom increase rather smoothly with the increase of cluster size N. For comparison, we also displayed those lowest-energy clusters (Ge_{21}–Ge_{25}) reported by Wang *et al.*[23] with the cluster notation ge21-ntb to ge25-ntb. As shown in Table I, the NTB global minima are typically 1–2 eV higher in energy than the corresponding lowest-energy isomers in family I or II, indicating that improved NTB parameters may be needed to accurately compute the PES of germanium clusters.

Some major structural differences between the low-lying germanium clusters and silicon counterparts in the size range of $21 \leq N \leq 29$ can be summarized as follows.

(1) The endohedral cagelike near-spherical clusters of family III are *not* energetically competitive compared to the prolate clusters in family I or II. Typically, near-spherical clusters are 0.7–2 eV higher in energy than the prolate counterparts, regardless of the DFT/PBE or DFT/BLYP calculations. In contrast, for neutral silicon clusters, near-spherical clusters become competitive in energy compared with the prolate isomers, starting from Si_{26}. To obtain low-energy near-spherical germanium clusters, we first set the initial structures of near-spherical germanium clusters to be the same as those of the lowest-energy silicon clusters.[17] We then performed BH/DFT-PBE search using 50 MC trials to obtain slightly improved local minima of near-spherical clusters. Still, we found that the prolated isomers are notably lower in energy than all the near-spherical isomers obtained. This result is consistent with the ion-mobility measurements in that the prolate-to-near-spherical structural transformation does not occur for germanium clusters until $N \sim 65$.[20]

(2) The Y-shaped three-arm clusters in family IV are *not* energetically competitive compared to the prolate clusters in family I or II. Only ge27-4a can be viewed as a low-lying isomer since DFT/BLYP calculation shows that it is only about 0.3 eV higher in energy than the lowest-energy isomer.
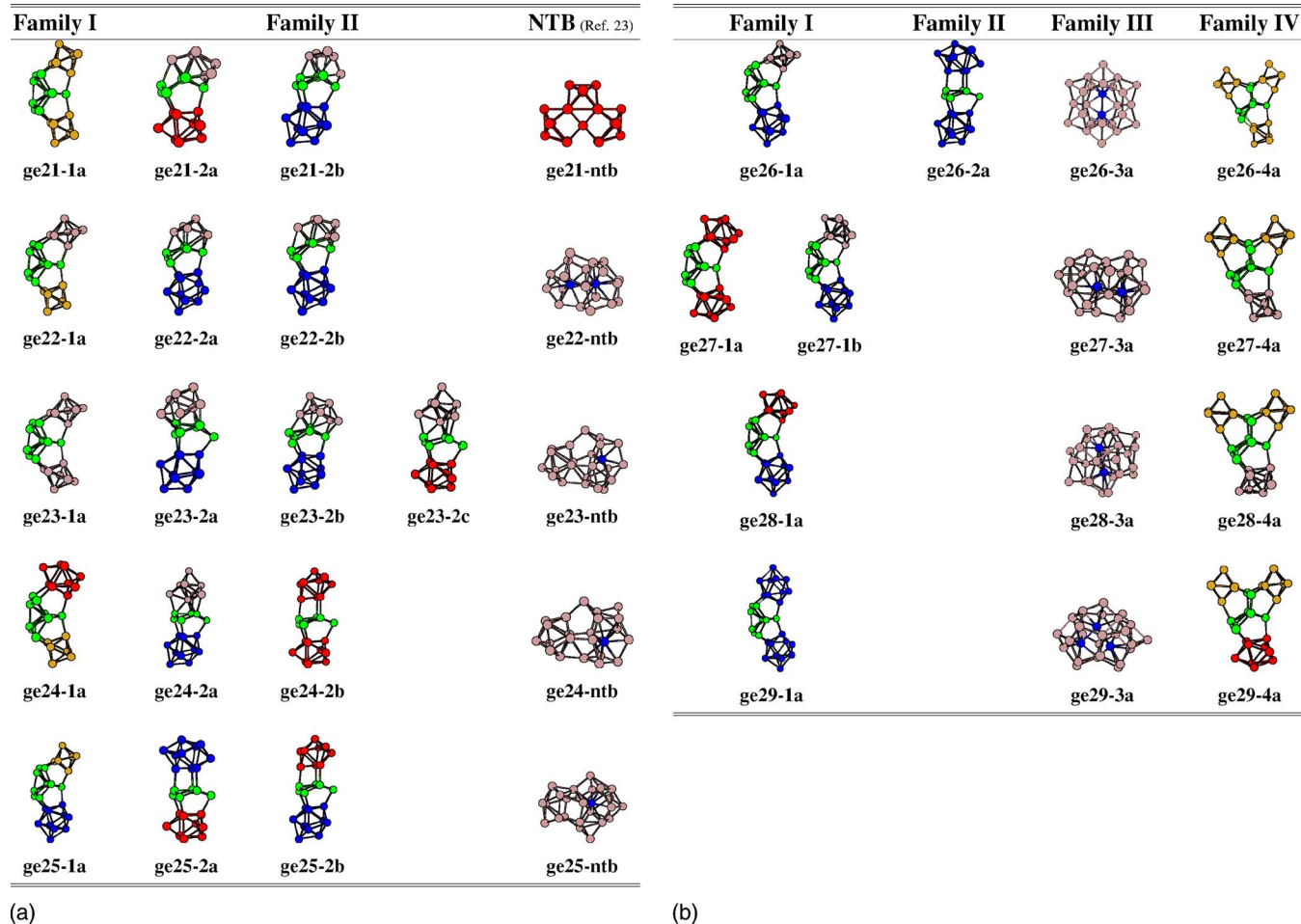
FIG. 2. (Color online) Low-energy clusters of (a) Ge_N ($21 \leq N \leq 25$) and (b) Ge_N ($26 \leq N \leq 29$) based on the constrained basin-hopping global search. The prolate clusters in families I and II as well as the "three-arm" clusters in family IV are built upon various generic structural motifs (Ref. 17). The puckered-hexagonal-ring Ge_6 unit and the fused-puckered-hexagonal-ring Ge_9 unit are highlighted in green. The *tetragonal bipyramid* Ge_6, *pentagonal bipyramid* Ge_7, TTP Ge_9, and *bicapped antiprism* Ge_{10} are highlighted in yellow, light-purple, red, and blue, respectively. For endohedral cagelike clusters, the endohedral atoms are highlighted in blue. The notation **1a** refers to the isomer that has the lowest energy (DFT/PBE calculation) in family I and the notation **1b** refers to the isomer that has the second lowest-energy in family I. The lowest-energy germanium clusters obtained based on the NTB calculations (Ref. 23) are also displayed in (a).

(3)   Among the prolate clusters in families I and II, DFT/PBE calculation favors the family II clusters ($Ge_{21}-Ge_{26}$) which all contain either a TTP motif or a Ge_{10} motif. For Ge_{21} and Ge_{25} DFT/BLYP calculation suggests that clusters ge21-1a and ge25-1a in family I are the lowest-energy clusters. These results are consistent with those of silicon clusters[7,17] in that DFT/BLYP total-energy calculation slightly favors the six/six motif whereas DFT/PBE calculation favors the TTP motif. Note that because of the intrinsic error bar of DFT total-energy calculation (typically within 5 meV/atom in binding energy per atom for semiconductor clusters), we can view that those isomers with the energy difference from the lowest-energy isomer less than 0.1 eV (see Table I) are isoenergetic with the lowest-energy isomer. In other words, these "isoenergetic" isomers can be all viewed as leading candidates for the global minimum. For example, ge22-2a and ge22-2b are isoenergetic, and so are ge23-2a, ge23-2b, and ge23-2c. Their energy differences are highlighted in bold in Table I.

(4)   The last main structural feature of the lowest- and low-lying germanium clusters is that several clusters with an odd number of atoms (ge21-2a, ge25-2a, and ge27-1a) contain the *six/nine* (Ge_6/Ge_9) motif in which the *nine*-atom subunit is the TTP unit. As a comparison, many silicon-cluster counterparts favor the *six/ten* (Ge_6/Ge_{10}) motif (except Si_{23}[17]). Similar conclusion has been made before for smaller germanium clusters,[2] that is, the TTP motif is strongly favored by the low-lying germanium clusters compared to the silicon clusters. For germanium clusters with an even number of atoms, the *six/ten* (Ge_6/Ge_{10}) structural motif is universally favored, as for the silicon clusters.

IV. CONCLUSION

We have performed a constrained global search for the geometries of low-lying germanium clusters in the size range of $21 \leq N \leq 29$. Because of the constrained search in nature, we cannot claim that the lowest-energy clusters obtained are the global minima. At present, we can only consider these

lowest-energy clusters as leading candidates for the global minimum since they are all appreciably lower in energy than those previously reported based on either NTB calculations or DFT calculations. Several distinct structural features of the germanium clusters are identified and their main differences from the silicon cluster in the same size range are discussed. First and foremost, the endohedral cagelike near-spherical germanium clusters are not energetically competitive in this size range. In other words, the low-lying germanium clusters in the size range of $21 \leq N \leq 29$ are all prolate in shape. This result is consistent with the ion-mobility measurement in that medium-sized clusters detected are prolate in shape for $N < 65$. Second, the *six/nine* motif—a puckered-hexagonal-ring Ge_6 unit attached to a tricapped trigonal prism Ge_9—is strongly favored by low-lying germanium clusters with an odd number of atoms, whereas the *six/ten* motif is universally favored by the germanium clusters with an even number of atoms. In contrast, many low-lying silicon clusters favor the six/six motif, rather than the *six/nine* motif. One way to confirm the existence of these generic structural motifs is to compare simulated anion photoelectron spectra and photoionization thresholds with the measured ones,[41] as recently done for silicon clusters.[16] Such a joint experimental/theoretical effort is underway.

ACKNOWLEDGMENTS

[1] A. A. Shvartsburg, B. Liu, Z.-Y. Lu, C.-Z. Wang, M. F. Jarrold, and K.-M. Ho, Phys. Rev. Lett. **83**, 2167 (1999).

[2] S. Bulusu, S. Yoo, and X. C. Zeng, J. Chem. Phys. **122**, 164305 (2005).

[3] K.-M. Ho, A. A. Shvartsburg, B. Pan, Z.-Y. Lu, C.-Z. Wang, J. G. Wacker, J. L. Fye, and M. F. Jarrold, Nature (London) **392**, 582 (1998).

[4] S. Yoo and X. C. Zeng, Angew. Chem., Int. Ed. **44**, 1491 (2005).

[5] I. Rata, A. A. Shvartsburg, M. Horoi, Th. Frauenheim, K. W. Michael Siu, and K. A. Jackson, Phys. Rev. Lett. **85**, 546 (2000).

[6] S. Goedecker, W. Hellmann, and T. Lenosky, Phys. Rev. Lett. **95**, 055501 (2005).

[7] S. Yoo and X. C. Zeng, J. Chem. Phys. **123**, 164303 (2005).

[8] L. Mitas, J. C. Grossman, I. Stich, and J. Tobik, Phys. Rev. Lett. **84**, 1479 (2000).

[9] B.-X. Li, P.-L. Cao, and S.-C. Zhan, Phys. Lett. A **316**, 252 (2003); B.-X. Li, Phys. Rev. B **71**, 235311 (2005).

[10] A. Sieck, Th. Frauenheim, and K. A. Jackson, Phys. Status Solidi B **240**, 537 (2003).

[11] S. Yoo, X. C. Zeng, X. Zhu, and J. Bai, J. Am. Chem. Soc. **125**, 13318 (2003).

[12] S. Yoo, J. J. Zhao, J. L. Wang, and X. C. Zeng, J. Am. Chem. Soc. **126**, 13845 (2004).

[13] K. A. Jackson, M. Horoi, I. Chaudhuri, Th. Frauenheim, and A. A. Shvartsburg, Phys. Rev. Lett. **93**, 013401 (2004).

[14] A. A. Shvartsburg, M. Horoi, and K. A. Jackson, *Spectroscopy of Emerging Materials* (Kluwer, Dordrecht, 2004).

[15] O. Guliamov, L. Kronik, and K. A. Jackson, J. Chem. Phys. **123**, 204312 (2005).

[16] J. Bai, L.-F. Cui, J. L. Wang, S. Yoo, X. Li, J. Jellinek, C. Koehler, T. Frauenheim, L.-S. Wang, and X. C. Zeng, J. Phys. Chem. A **110**, 908 (2006).

[17] S. Yoo and X. C. Zeng, J. Chem. Phys. **124**, 054304 (2006).

[18] M. F. Jarrold and V. A. Constant, Phys. Rev. Lett. **67**, 2994 (1991).

[19] A. A. Shvartsburg, R. R. Hudgins, P. Dugourd, and M. F. Jarrold, Chem. Soc. Rev. **30**, 26 (2001).

[20] J. M. Hunter, J. L. Fye, M. F. Jarrold, and J. E. Bower, Phys. Rev. Lett. **73**, 2063 (1994).

[21] A. P. Alivisatos, Science **271**, 933 (1996).

[22] C. Jo and K. Lee, J. Chem. Phys. **113**, 7268 (2000).

[23] J. Wang, G. Wang, and J. Zhao, Phys. Rev. B **64**, 205411 (2001).

[24] F.-S. Liang and B.-X. Li, Phys. Lett. A **328**, 407 (2004).

[25] J. Wang, M. Yang, G. H. Wang, and J. J. Zhao, Chem. Phys. Lett. **367**, 448 (2003).

[26] D. J. Wales and J. P. K. Doye, J. Phys. Chem. A **101**, 5111 (1997).

[27] J. P. K. Doye and D. J. Wales, Phys. Rev. Lett. **80**, 1357 (1998).

[28] J. P. K. Doye, M. A. Miller, and D. J. Wales, J. Chem. Phys. **110**, 6896 (1999).

[29] D. J. Wales, Science **271**, 925 (1996).

[30] D. J. Wales and M. P. Hodges, Chem. Phys. Lett. **286**, 65 (1998).

[31] D. J. Wales, M. A. Miller, and T. R. Walsh, Nature (London) **394**, 758 (1998).

[32] D. J. Wales and H. A. Scheraga, Science **285**, 1368 (1999).

[33] D. J. Wales, *Energy Landscapes with Applications to Clusters, Biomolecules and Glasses* (Kluwer, Berlin, 2004).

[34] J. Perdew, K. Burke, and M. Ernzerhof, Phys. Rev. Lett. **77**, 3865 (1996).

[35] A. D. Becke, Phys. Rev. A **38**, 3098 (1988); C. Lee, W. Yang, and R. G. Parr, Phys. Rev. B **37**, 785 (1988).

[36] J. Hutter, A. Alavi, T. Deutsch, M. Bernasconi, S. Goedecker, D. Marx, M. Tuckerman, and M. Parrinello, CPMD, Version 3.7.1, MPI für Festkörperforschung, Stuttgart, 1997–2001.

[37] D. Hamann, Phys. Rev. B **40**, 2980 (1989).

[38] N. Troullier and J. L. Martins, Phys. Rev. B **43**, 1993 (1991).

[39] L. Kleinman and D. M. Bylander, Phys. Rev. Lett. **48**, 1425 (1982).

[40] S. Ogöt and J. R. Chelikowsky, Phys. Rev. B **55**, R4914 (1997).

[41] S. Yoshida and K. Fuke, J. Chem. Phys. **111**, 3880 (1999).